Organic & Biomolecular Chemistry

Cite this: *Org. Biomol. Chem.*, 2011, **9**, 689

www.rsc.org/obc

PAPER

How reliable are DFT transition structures? Comparison of GGA, hybrid-meta-GGA and meta-GGA functionals†

Luis Simón*[a] and Jonathan M. Goodman*[b]

Received 22nd July 2010, Accepted 14th September 2010
DOI: 10.1039/c0ob00477d

There have been many comparisons of computational methods applied to ground states, but studies of organic reactions usually require calculations on transition states, and these provide a different test of the methods. We present calculations of the geometries of nineteen covalent-bond forming transition states using HF and twelve different functionals, including GGA, hybrid-GGA and hybrid meta-GGA approaches. For the calculation of the TS geometries, the results suggest that B3LYP is only slightly less accurate than newer, computationally more expensive methods, and is less sensitive to choice of integration grid. We conclude that the use of B3LYP and related functionals is still appropriate for many studies of organic reaction mechanisms.

Introduction

The development of the Kohn–Sham approach to DFT[1,2] and the availability of powerful computers are responsible for the dramatic increase in the number of applications of molecular electronic structure calculations to problems in organic chemistry. Among these applications, the search for transition state structures is one of the most interesting for two reasons: first, transition state searches can be used to test hypotheses about reaction mechanisms; second, even though femtosecond spectroscopy can detect extremely short living reaction intermediates,[3] there is no experimental procedure which allows the direct observation of these structures.

Part of the success of DFT methods arises from the constant development of new functionals that overcome the imperfections of earlier generations. Early functionals used the local density approximation (LDA) which worked well, in part because of the cancellation of errors from different approximations. The generalized gradient approximation (GGA) uses a more complex, and, therefore, slower set of equations, but which delivered greater precision. With the development of hybrid functionals, which combine the GGA and exact exchange, and, in particular, with the development of the popular B3LYP[4,5] functional, computational chemistry found a method which combine a high degree of accuracy while requiring computational resources only slightly higher than Hartree–Fock methods. B3LYP has become a standard in quantum chemistry calculations, and many notable contributions to the determination of reaction mechanisms by computational methods use this functional.

Nevertheless, recent reports question the reliability[6–9] of B3LYP functional. It has been pointed out that this functional incorrectly predicts the reaction energies of homolytic bond breaking reactions,[10,11] reactions involving transformation between σ and π bonds,[12–14] isomerism between linear and branched organic compounds and silanes[13,15–18] and other isodesmic reactions.[19] The error increases with the number of bonds in the molecule,[16] and might be caused by deficiencies in the treatment of medium-range interactions[17,20] and of proto-branching effects.[6,15,16,18] Substantial errors have also been found in the description of non-bonding and long-range interactions.[7,21,22] Luckily, more recent functionals (such as meta-GGA functionals,[8,23–27] double-hybrid functionals[28–30] and functionals containing long-range dispersion corrections[29–32]) reduce these problems considerably. Benchmark studies,[6–9,11–19,21–23,29,30,33–50] show that they offer more reliable results.

The uncertainty about the reliability of B3LYP and the development of new functionals that are both more accurate and more computationally expensive, have led to a reduction of in the use of B3LYP. This is illustrated by the recent reduction of the number of publications indexed in Sci-Finder database[51] with both the keywords "transition state" and "B3LYP" (Fig. 1).

Because the issues with B3LYP are now well known, and because modern functionals are now widely available, the choice of the most appropriate functional to use for the study of reaction mechanisms is a question gaining increasing prominence. Although

[a]*Facultad de Ciencias Químicas, Universidad de Salamanca, Plaza de los Caídos 1-5, Salamanca, E37004, Spain. E-mail: lsimon@usal.es; Tel: +34 (0) 675158937*

[b]*Unilever Centre For Molecular Science Informatics, Department of Chemistry, Lensfield Road, Cambridge, UK., CB2 1EW. E-mail: jmg11@cam.ac.uk; Fax: +44 (0)1223 763076; Tel: 44 (0)1223 336434*

† Electronic supplementary information (ESI) available: Full list of authors in Gaussian03 reference. Relative computational cost of each method. Cartesian coordinates of the structures optimized by M05(-2X) functional (ultrafine grid). Comparison with experimental data for jo78, jo15, ja20, jo8a, ja37, an02 and jo5k reactions. Frequencies at which the RMSD differences were higher than 0.2 Å, 0.3 Å and 0.4 Å. Frequencies at which the maximum deviations distances of bonds forming (or breaking) in the TS were higher than 0.1 Å, 0.2 Å and 0.4 Å. Times that maximum dihedral angle deviations were higher than 30°, 60° and 90°. Deviations of geometrical parameters (.xls file). See DOI: 10.1039/c0ob00477d

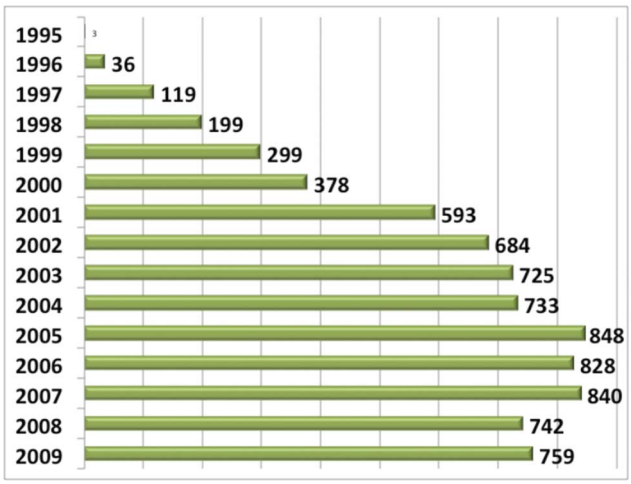

Fig. 1 Number of papers published each year with both keyword: "transition state" and "B3LYP" (data from Sci-Finder).

many recent papers study the accuracy of DFT functionals, these have focused on analyses of ground states, because these are most easily related to experimental data. However, it is not clear that the best functionals for ground states will also be the best functionals to describe transition states. In addition, whilst more sophisticated functionals should offer more reliable transition state geometries and energies, the computer time required will also be higher. It is, therefore, important to study whether or not the benefit of the most recent functionals justifies their computational cost in "real-life" transition structure calculations. Previous DFT benchmark studies, on ground states do not allow us to draw firm conclusions on this question for the following reasons:

(1) Many DFT functional benchmarks studies are based on single-point calculations on fixed geometries. In some cases, the geometries are optimized using extremely high level of theory.[7,8,21,36,52] This approach is very useful in establishing a comparison of different functionals and theoretical methods, but reflects an unrealistic scenario, because if the high-level calculations are available, it would not make sense to perform single-point calculations with a cheaper and less reliable DFT method. Transition state searches are usually computationally demanding as a result of the complexity of the potential energy surfaces that need to be investigated, and so such high levels of theory cannot usually be afforded.

(2) When identical geometries are used in the benchmarks, the functionals' ability to provide good geometries is not tested. A method that yields imprecise energies can still be useful if it also produces reliable transition state geometries, since it is common practice to use different levels of theory for optimization and final single-point energy evaluation. Most of the computational (and human) effort required in the calculation is used in the geometry optimization step, so the overall computing time would be considerably reduced if a cheaper method could be used for this process. Except in some cases,[28,37,39,42,47–49,52] the geometries obtained by different functionals are not compared.

(3) Large basis sets are usually used in the comparison of functionals. As with the use of high quality geometries, this choice is reasonable because the resulting benchmark will not reflect the sensitivity of the functional to the use of incomplete basis sets.[45,53–57] In real applications, however, basis set choice is limited by the need to complete the calculation within a reasonable time. As a result, the error resulting from the use of incomplete basis sets could be more important than the intrinsic functional error.

(4) In many cases, transition state searches are used to discriminate between several possible mechanisms, so the alternative transition states have identical number of atoms and similar bonding patterns. Good examples are relevant mechanistic studies on enantioselective reactions, where mechanistic proposals are tested based on the ability of diastereomeric transition state energies to reproduce experimental results. Many of the sources of error in the use of older functionals (such as cumulative errors, or the impossibility of describing medium-range interactions and proto-branching) might cancel in the calculation of energy differences of similar transition state structures.[20]

In this paper, we address all of these issues, by testing the ability of different functionals to reproduce the energy differences between pairs of competing transition state structures and the quality of the geometries obtained with these functionals. We have studied pairs of competing transition states of reactions that have already been studied by computational methods. Our goal is not to establish an absolute benchmark of the different functionals, but rather to assess how the choice of functional influences the results of these studies.

Results and discussion

Dependence of $\Delta\Delta E^{\ddagger}$ and $\Delta\Delta G^{\ddagger}$ on the functional used

We have gathered nineteen examples of selective organic reactions from the recent literature. For each reaction, we have used two different transition state structures that correspond to competing mechanisms. The structures are shown in Fig. 2. This set is representative of the type of organic and organometallic reaction mechanisms now being studied using computational methods, and, although it is impossible to include all possibilities in the study, the set covers many types of reactions and a range of molecular sizes. The initial transition structures for the calculations were taken from the cartesian coordinates in the supporting information of the original studies. In all cases the geometries were re-optimized with different functionals using the same basis set as the original publications (Fig. 2). Each reaction is identified by the two first and two last letters of the DOI of the original publication, and the name of each structure is consistent with that used in the supporting information section.

We first studied the difference in the gas-phase single-point energy ($\Delta\Delta E^{\ddagger}$) and the difference in the Gibbs free energy at 298.15 K ($\Delta\Delta G^{\ddagger}$) for each of the 19 pairs of competing transition states using HF, B3LYP[5,59,62] and M05-2X[68] (for the transition state structures with no transition metal atoms) or M05[41,69] (for the transition state structures with a transition metal). All calculations were performed using Gaussian03 rev. E program.[58] For those structures with a multiplicity of more than one, unrestricted calculations were performed; the remaining transition structures were obtained using the restricted closed shell methods. The default Gaussian03 pruned 75302 grid (75 radial shells and 302 angular points per shell) was used for numerical integration, but we also used the pruned 99590 grid (ultrafine grid in Gaussian03, keyword: integral = grid = ultrafine) for the M05(-2X) functional

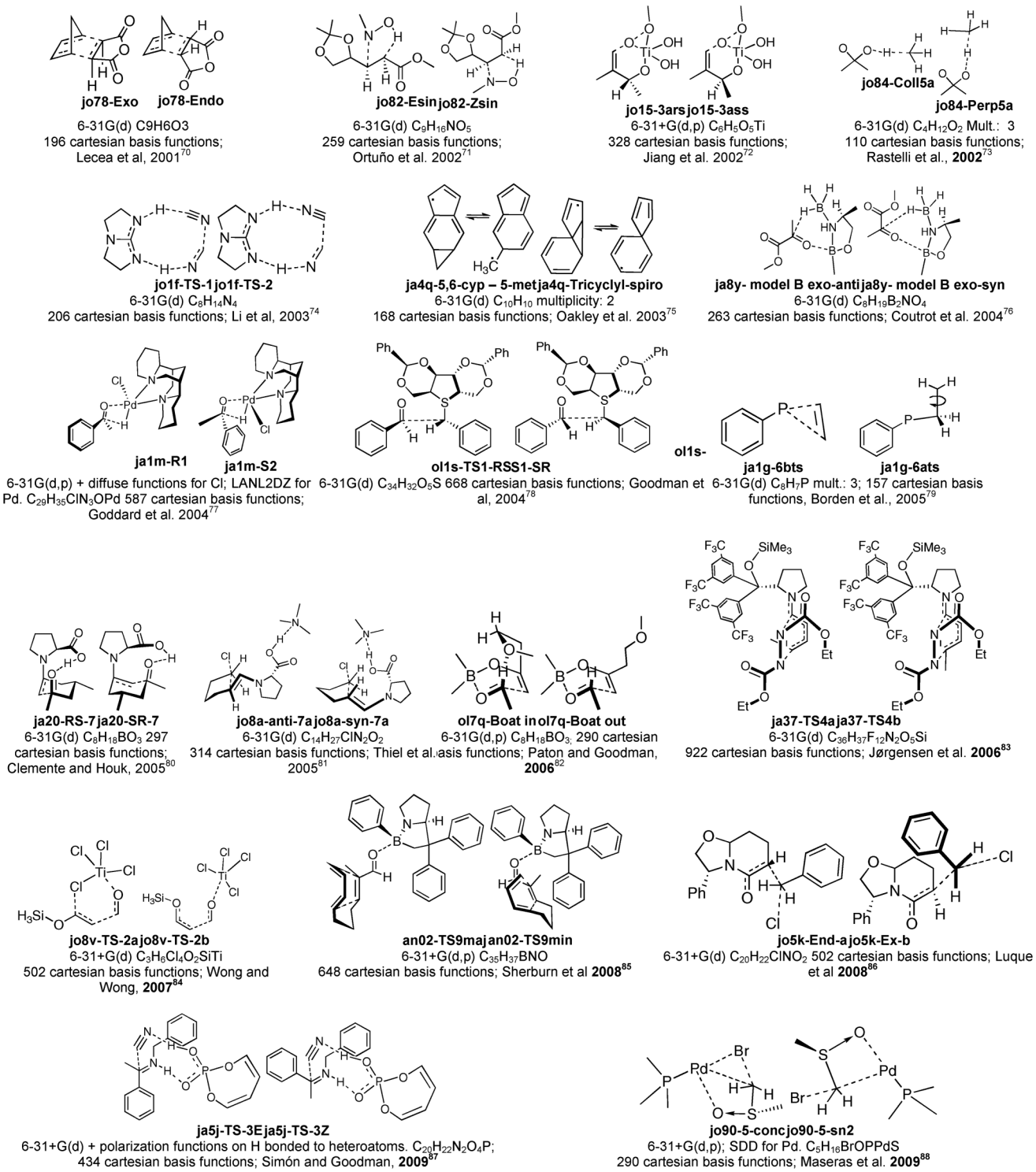

Fig. 2 The transition structures included in the test set. The basis set, molecular formula, number of Cartesian basis functions and reference are all shown.[70-88]

(abbreviated as M05-2X-UF). The results are summarised in Fig. 3, which illustrates the differences in $\Delta\Delta E^{\ddagger}$ and $\Delta\Delta G^{\ddagger}$ with between HF, B3LYP and M05-2X and the results using M05-2X with an ultrafine grid (M05-2X-UF). Each transition state had just one imaginary frequency. These frequencies were method dependent, but all functionals gave mean results between 98% and 136% of the M-05-2X-UF result. Fig. 4 compares the calculations with experimental data, in the cases for which these are available.

A number of HF and B3LYP calculations show rather different results to M05-2X-UF in both $\Delta\Delta E^{\ddagger}$ and $\Delta\Delta G^{\ddagger}$ (for example, jo90, ja4q or ja37, Fig. 3). This demonstrates the importance of the choice of the functional in studies of organic reaction mechanisms.

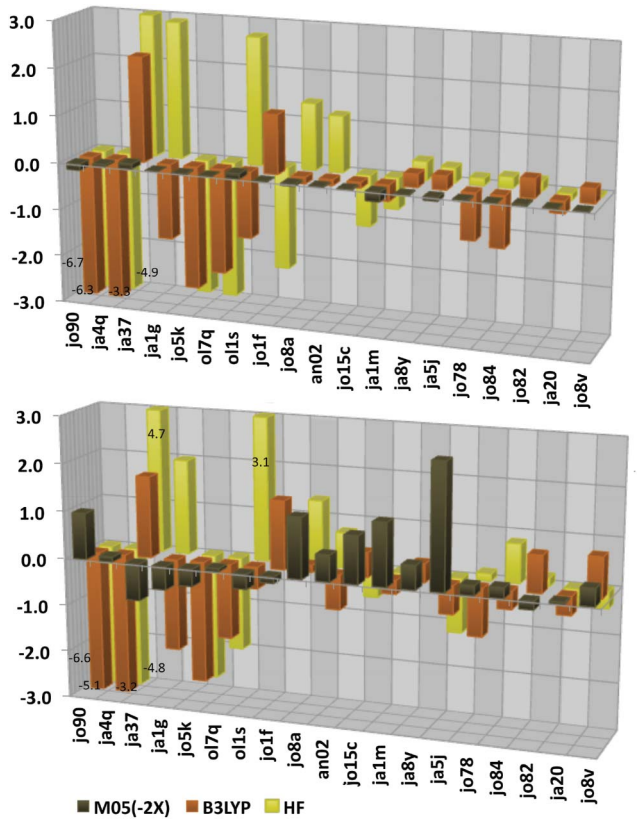

Fig. 3 Comparison of $\Delta\Delta E^{\ddagger}$ (top) and $\Delta\Delta G^{\ddagger}$ (bottom) for each pair of competing transition states with respect to values obtained with M05(-2X)-UF (kcal/mol).

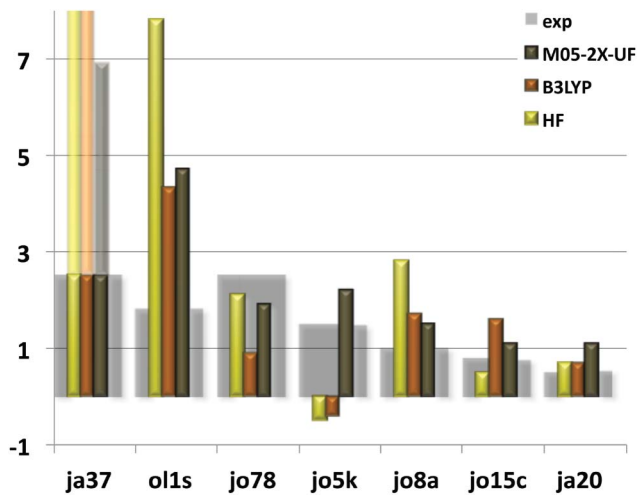

Fig. 4 Comparison of $\Delta\Delta G^{\ddagger}$ calculated with the values obtained from the experiments.

The differences between the standard and ultrafine grid are small for $\Delta\Delta E^{\ddagger}$ using the M05(-2X) functional, but for $\Delta\Delta G^{\ddagger}$ they are remarkably large in some cases (for example, ja5j, ja1m, or jo8a, Fig. 3).

Fig. 4 shows how the different functionals related to experimental data in those cases for which an experimental energy difference can be estimated. In nearly all combinations of functional and reaction, the sense of the selectivity is assigned correctly. We do not expect quantitative agreement between the calculations and the experiments because this study compares just two transition structures for each case, and other pathways may also contribute to the product ratios. In addition, our study compares the gas-phase results of the functionals, and so does not take into account the influences of solvents on the experiments. In some cases, the authors of the studies listed in Fig. 2 simplified the molecules used in the experiments in order to make the calculations more tractable, and we based our calculations on their methodology. For all these reasons, the comparison with the experimental values should not be taken as an absolute benchmark of the functionals. Fig. 4 shows $\Delta\Delta G^{\ddagger}$ calculated with HF, B3LYP and M05(-2X)-UF methods, compared with the values estimated from the experimental results for ja20, jo15, jo8a, jo5k, an02, jo78 and ja37. In one case (jo5k), only M05(-2X)-UF gives the correct enantioselectivity, and both HF and B3LYP suggest very low selectivity with the opposite sense. This reaction is an acyclic nucleophilic substitution and so the result selectivity depends entirely on medium-range interactions across the single forming bond. In every other case the transition states have some cyclic character, except jo84 for which the reactant (methane) is highly symmetrical. As a result, jo5k is expected to be a particularly challenging reaction to model accurately.

On the basis of these initial results, which confirm that the results obtained from computational studies in organic reaction mechanism are highly dependant on the functional used, we extended the study to include more functionals: pure GGA functionals (BLYP,[5,59] HCTH407[53,60,61]); hybrid GGA functionals (B3P86,[4,5,59] B3PW91,[4,59] O3LYP[5,63,64], PBE1PBE,[65,66] BHandHLYP[5,59] as defined in the Gaussian03 program: $0.5E_X^{HF} + 0.5E_X^{LSDA} + 0.5E_X^{Becke88}$), in addition to B3LYP; the hybrid meta-GGA functionals BMK[67] and MPWB1K[23] as well as M05(-2X). For both M05(-2X), B3LYP we included calculations with both the default grid and an ultrafine grid. Using the optimized structures, frequency calculations were performed at the same level of theory, and were used to calculate the Gibbs free energy of each structure at 298.15 K. All the calculations were performed in the gas phase. An estimate of the computational cost of each method was obtained from the time required for the calculation of the frequencies using analytic second derivatives on the optimized geometries (see the supporting information).

For each pair of competing transition state structures, the difference in the single-point energy ($\Delta\Delta E^{\ddagger}$), the difference in the zero-point energy ($\Delta\Delta zpE^{\ddagger}$), and the difference in the Gibbs free energy at 298.15 K ($\Delta\Delta G^{\ddagger}$) were calculated using each tested functional. The results are summarized in Fig. 5. Values deduced from the experimental results are also shown for those cases in which these could be calculated.

In order to help assess the data in Fig. 5, the differences in $\Delta\Delta E^{\ddagger}$ and $\Delta\Delta G^{\ddagger}$ values for each pair of functionals is shown in Fig. 6. The top-right triangle shows the average energy differences and the lower-left triangle the maximum absolute difference for the nineteen reactions. The intensity of the colours of each cell increases with the value in the cell: darker shades correspond to greater differences.

HF shows differences greater than 1 kcal/mol on average for $\Delta\Delta E^{\ddagger}$ and $\Delta\Delta G^{\ddagger}$, and the maximum differences are over 2.5 kcal/mol. The pure GGA functionals tested (BLYP and HCTH) and the hybrid GGA functionals (B3LYP, B3P86,

ΔΔE‡ kcal/mol	jo78	jo1f	jo84	ol7q	jo15c	ja8y	jo82	ja20	jo90	ja4q	ja1g	jo8v	jo8a	jo5k	ja5j	ja1m	an02	ol1s	ja37
HF	2.1	-1.7	3.3	0.9	0.0	1.6	1.6	1.7	-5.5	-0.2	10.1	1.3	2.7	0.1	2.0	1.4	2.0	8.0	10.3
BLYP	0.5	2.1	1.3	1.3	1.0	1.2	1.6	1.5	-4.9	0.6	1.8	2.9	0.7	0.0	1.9	1.6	0.6	3.1	8.0
HCTH	0.7	2.8	0.4	1.1	1.7	1.5	2.0	0.8	-2.9	2.3	3.4	1.6	1.1	-0.1	1.5	1.7	1.5	2.0	8.3
B3LYP	0.9	1.7	2.0	1.5	0.9	1.5	1.8	1.6	-5.1	1.4	5.6	1.6	1.1	0.4	2.0	1.7	0.7	3.9	8.6
B3LYP-UF	0.9	1.7	2.0	1.5	0.9	1.5	1.8	1.6	-5.0	1.4	5.6	1.7	1.2	0.4	2.0	1.7	0.7	4.0	8.7
B3P86	1.1	2.1	2.0	1.9	1.1	1.3	1.9	1.8	-4.8	2.8	7.9	1.3	1.3	1.0	2.2	2.2	0.4	4.4	8.4
B3PW91	1.1	2.2	2.0	1.3	1.2	1.5	2.0	1.6	-4.9	2.7	7.7	1.3	1.4	0.5	2.2	2.1	0.8	4.6	9.0
O3LYP	0.9	2.6	1.3	0.6	1.8	1.7	2.2	0.9	-4.3	2.7	5.6	1.0	1.5	-0.5	1.2	1.8	1.3	3.8	9.4
PBE1PBE	1.3	2.0	2.3	2.2	1.1	1.4	1.8	1.8	-4.0	3.3	9.1	1.2	1.4	1.0	1.4	2.4	0.6	7.1	8.3
BHANDHLYP	1.5	0.5	3.1	1.8	0.6	1.8	1.5	1.9	-4.4	1.6	10.0	1.3	1.7	0.6	2.1	1.8	0.8	5.1	9.0
BMK	1.5	0.6	2.8	2.4	0.7	2.1	2.2	2.6	-1.9	4.7	9.8	1.9	0.9	2.4	2.3	2.1	-0.2	4.7	6.8
MPWB1K	1.8	1.2	-2.9	2.6	1.0	1.6	2.1	2.2	-1.6	4.8	1.7	2.9	1.5	3.4	1.1	3.3	0.3	5.5	7.3
M05-2X	1.9	0.5	3.1	3.7	1.0	1.2	1.4	1.8	1.1	4.8	7.2	1.3	1.2	3.0	1.6	1.9	0.8	5.4	6.5
M05-2X-UF	1.9	0.5	3.1	3.7	1.0	1.2	1.4	1.9	1.2	4.7	7.2	1.3	1.3	3.0	1.7	2.1	0.8	5.3	6.4

ΔΔz.p.E‡ kcal/mol	jo78	jo1f	jo84	ol7q	jo15c	ja8y	jo82	ja20	jo90	ja4q	ja1g	jo8v	jo8a	jo5k	ja5j	ja1m	an02	ol1s	ja37
HF	2.1	-1.7	3.3	0.9	0.0	1.6	1.6	1.7	-5.5	-0.2	10.1	1.3	2.7	0.1	2.0	1.4	2.0	8.0	10.3
BLYP	0.5	2.1	1.3	1.3	1.0	1.2	1.6	1.5	-4.9	0.6	1.8	2.9	0.7	0.0	1.9	1.6	0.6	3.1	8.0
HCTH	0.7	2.8	0.4	1.1	1.7	1.5	2.0	0.8	-2.9	2.3	3.4	1.6	1.1	-0.1	1.5	1.7	1.5	2.0	8.3
B3LYP	0.9	1.7	2.0	1.5	0.9	1.5	1.8	1.6	-5.1	1.4	5.6	1.6	1.1	0.4	2.0	1.7	0.7	3.9	8.6
B3LYP-UF	0.9	1.7	2.0	1.5	0.9	1.5	1.8	1.6	-5.0	1.4	5.6	1.7	1.2	0.4	2.0	1.7	0.7	4.0	8.7
B3P86	1.1	2.1	2.0	1.9	1.1	1.3	1.9	1.8	-4.8	2.8	7.9	1.3	1.3	1.0	2.2	2.2	0.4	4.4	8.4
B3PW91	1.1	2.2	2.0	1.3	1.2	1.5	2.0	1.6	-4.9	2.7	7.7	1.3	1.4	0.5	2.2	2.1	0.8	4.6	9.0
O3LYP	0.9	2.6	1.3	0.6	1.8	1.7	2.2	0.9	-4.3	2.7	5.6	1.0	1.5	-0.5	1.2	1.8	1.3	3.8	9.4
PBE1PBE	1.3	2.0	2.3	2.2	1.1	1.4	1.8	1.8	-4.0	3.3	9.1	1.2	1.4	1.0	1.4	2.4	0.6	7.1	8.3
BHANDHLYP	1.5	0.5	3.1	1.8	0.6	1.8	1.5	1.9	-4.4	1.6	10.0	1.3	1.7	0.6	2.1	1.8	0.8	5.1	9.0
BMK	1.5	0.6	2.8	2.4	0.7	2.1	2.2	2.6	-1.9	4.7	9.8	1.9	0.9	2.4	2.3	2.1	-0.2	4.7	6.8
MPWB1K	1.8	1.2	-2.9	2.6	1.0	1.6	2.1	2.2	-1.6	4.8	1.7	2.9	1.5	3.4	1.1	3.3	0.3	5.5	7.3
M05-2X	1.9	0.5	3.1	3.7	1.0	1.2	1.4	1.8	1.1	4.8	7.2	1.3	1.2	3.0	1.6	1.9	0.8	5.4	6.5
M05-2X-UF	1.9	0.5	3.1	3.7	1.0	1.2	1.4	1.9	1.2	4.7	7.2	1.3	1.3	3.0	1.7	2.1	0.8	5.3	6.4

ΔΔG‡ kcal/mol	jo78	jo1f	jo84	ol7q	jo15c	ja8y	jo82	ja20	jo90	ja4q	ja1g	jo8v	jo8a	jo5k	ja5j	ja1m	an02	ol1s	ja37
HF	2.1	-0.8	2.9	0.0	0.5	1.0	1.5	0.7	-6.4	-0.8	9.7	0.6	2.8	-0.5	1.5	1.3	2.4	7.8	11.6
BLYP	0.3	1.0	1.8	0.2	1.3	1.2	1.6	0.8	-5.0	0.1	2.0	2.1	1.2	-0.1	1.2	0.9	1.3	3.7	8.0
HCTH	0.0	1.3	1.3	0.3	1.6	1.5	2.2	0.4	-3.0	1.6	3.6	1.9	1.7	-0.5	1.9	0.9	1.9	3.3	8.9
B3LYP	0.9	0.7	1.7	0.4	1.6	1.3	2.1	0.7	-5.0	0.8	5.8	1.8	1.6	-0.4	2.1	1.3	0.9	4.3	8.6
B3LYP-UF	1.0	0.6	1.3	0.4	1.4	0.9	0.6	0.7	-5.8	0.9	5.7	1.5	1.5	-0.2	2.0	1.6	1.7	4.3	8.7
B3P86	1.2	0.8	1.5	0.5	1.6	0.7	1.5	0.8	-4.8	2.2	8.0	1.4	1.6	-0.3	2.6	2.4	0.9	5.0	8.4
B3PW91	1.1	0.8	1.6	0.2	1.8	0.8	1.9	0.7	-4.9	2.1	7.8	1.2	1.5	-0.3	1.5	2.2	0.7	5.2	8.6
O3LYP	0.8	1.2	1.1	-0.3	1.9	1.3	2.3	0.3	-4.3	2.1	5.7	0.7	1.5	-1.1	1.2	1.4	1.5	4.8	8.9
PBE1PBE	1.3	0.7	1.9	0.8	1.7	0.8	1.1	0.8	-4.2	2.7	9.2	1.2	1.6	-0.1	3.3	2.8	1.1	4.8	8.4
BHANDHLYP	1.5	-0.2	2.8	0.7	1.6	1.0	1.6	0.8	-4.8	0.9	9.9	1.3	2.1	-0.1	1.8	1.6	1.3	6.2	9.1
BMK	1.6	-0.2	2.4	1.6	0.9	2.6	1.3	2.6	-3.4	4.0	10.4	-0.3	1.4	-0.4	4.2	1.7	-0.2	4.7	8.8
MPWB1K	1.7	-0.3	2.6	1.0	2.4	1.4	1.5	0.6	-2.9	4.2	3.2	1.8	1.4	2.9	1.0	2.9	2.2	6.3	7.2
M05-2X	2.1	-0.9	3.3	2.0	2.1	1.4	1.1	1.1	1.1	4.2	7.2	1.4	2.7	1.8	5.3	2.9	2.2	4.4	6.1
M05-2X-UF	1.9	-0.8	2.1	1.9	1.1	0.9	1.3	1.1	0.1	4.1	7.7	1.0	1.5	2.2	2.7	1.6	1.7	4.7	6.9
exp	>2.5				0.8			0.5					1.0	1.5				1.8	>2.5

Fig. 5 $\Delta\Delta E^{\ddagger}$ (top), $\Delta\Delta zpE^{\ddagger}$ (middle) and $\Delta\Delta G^{\ddagger}$ (bottom) for each pair of competing transition state. Energies are in kcal/mol.

B3PW91, PBE1PBE, O3LYP and BHandHLYP) give similar average results within this group, but some individual differences in $\Delta\Delta E^{\ddagger}$ and $\Delta\Delta G^{\ddagger}$ are high, as shown by the maximum absolute values. Both average and maximum absolute differences in $\Delta\Delta E^{\ddagger}$ and $\Delta\Delta G^{\ddagger}$ increase when these functionals are compared with hybrid meta-GGA functionals (BMP, MPWB1K and M05(-2X)).

Importance of the integration grid

As already shown in Fig. 3 (top) or Fig. 6 (top), the use of ultrafine grid has only a very small effect on the calculated $\Delta\Delta E^{\ddagger}$ and $\Delta\Delta zpE^{\ddagger}$ values show a similar trend. Wheeler and Houk have studied the integration grid errors in a set of reactions for GGA and meta-GGA functionals.[89] In agreement with our results, they found that the standard grid in Gaussian03 gives small deviations when compared with much finer integration grids for M05-2X functional. This is an important observation, since the use of the ultrafine grid nearly doubles the computational costs. However, the average and maximum differences in $\Delta\Delta G^{\ddagger}$ reveal that the grid can affect the calculation of the Gibbs free energy (see also Fig. 3, bottom). In the case of B3LYP functional, in only three cases the $\Delta\Delta G^{\ddagger}$ differences were higher than 0.5 kcal/mol (jo82, 1.5 kcal/mol, jo90, 0.8 kcal/mol, and an02, 0.7 kcal/mol). For the M05(-2X) functional, the $\Delta\Delta G^{\ddagger}$ differences between the ultrafine and the standard grid were higher than 0.5 kcal/mol in eight different reactions (ja5j, 2.6 kcal/mol; ja1m, 1.3 kcal/mol;

Table 1 Comparison of absolute differences in $\Delta\Delta G^{\ddagger}$ for each reaction obtained with the standard and the ultrafine grids and the absolute differences in the vibrational term of $T\Delta\Delta S^{\ddagger}$ at T = 298.15 K (all values in kcal/mol)

		jo78	jo1f	jo84	ol7q	jo15c	ja8y	jo82	ja20	jo90	ja4q	ja1g	jo8v	jo8a	jo5k	ja5j	ja1m	an02	ol1s	ja37
B3LYP	$T\Delta\Delta S^{\ddagger}_{vib}$	0.1	0.1	0.4	0.0	0.2	0.2	0.1	0.0	0.8	0.0	0.1	0.4	0.2	0.6	0.0	0.3	0.6	0.0	0.5
	$\Delta\Delta G^{\ddagger}$	0.2	0.1	0.4	0.0	0.2	0.3	0.2	0.0	0.8	0.0	0.1	0.3	0.1	0.2	0.0	0.2	0.7	0.0	0.1
M05(-2X)	$T\Delta\Delta S^{\ddagger}_{vib}$	0.3	0.1	1.6	0.3	0.9	0.4	0.3	0.0	0.9	0.0	0.4	0.6	1.1	0.5	1.2	1.0	1.2	0.3	1.2
	$\Delta\Delta G^{\ddagger}$	0.2	0.1	1.0	0.1	1.0	0.5	0.2	0.0	1.0	0.1	0.5	0.4	1.3	0.4	0.5	1.3	0.6	0.3	0.8

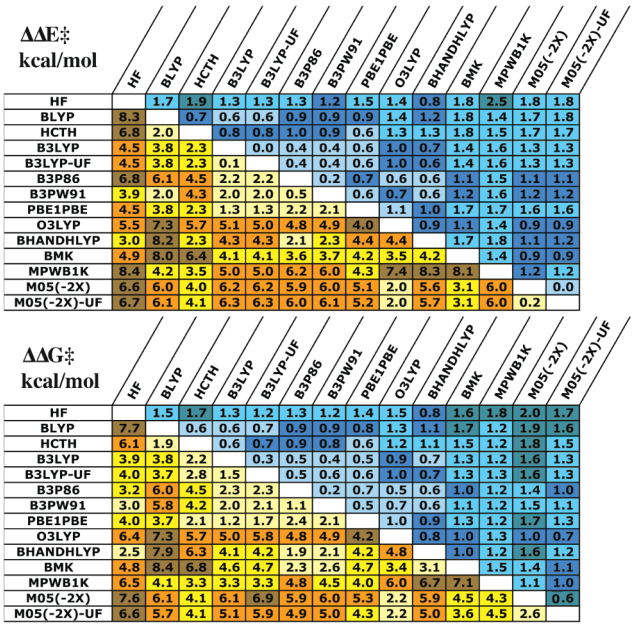

Fig. 6 Average (top-right of each table) and maximum (bottom-left of each table) absolute differences between $\Delta\Delta E^{\ddagger}$ (top) and $\Delta\Delta G^{\ddagger}$ (bottom) values calculated with each functional. The colours indicate the size of the differences, with the lightest colours indicating the closest agreements.

ja37, 0.8 kcal/mol; jo8a, 1.3 kcal/mol; jo15c, 1.0 kcal/mol; jo90, 1.0 kcal/mol; jo84, 1 kcal/mol, and an02, 0.5 kcal/mol). This confirms that M05(-2X) has a higher sensitivity to the integration grid than B3LYP. Most of this difference in $\Delta\Delta G^{\ddagger}$ for M05(-2X) when standard and ultrafine grids are used can be ascribed to different values of the vibrational contribution to the entropy. When absolute differences in this quantity obtained with standard and ultrafine grids were multiplied by the temperature (298.15 K), the energy obtained is very similar to the absolute differences in $\Delta\Delta G^{\ddagger}$ (see Table 1).

Scuseria[90] observed that frequencies calculated with standard grid often show spurious imaginary frequencies with meta-GGA functionals. We have observed that four M05-2X (ol1s, jo84, ja5j and an02) and three BMK (jo82, jo78, ja37) optimized transition structures showed two imaginary frequencies. The extremely large difference of $\Delta\Delta G^{\ddagger}$ with the standard and ultrafine grid for the ja5j reaction (2.6 kcal/mol for M05-2X) could be linked to the presence of the second imaginary frequency, but this is not the case of the rest of the reactions in which large differences were observed. Therefore, problematic cases cannot be detected by the presence of spurious imaginary frequencies. The results suggest that in those cases for which $\Delta\Delta E^{\ddagger}$ is not sufficient and the calculation of the Gibbs free energy is essential, meta-GGA functionals should only be used in combination with an ultrafine grid. This implies that the geometry optimization should be carried out using this grid, which will considerably increase the computational cost.

Comparison of the transition state geometries

The differences in the $\Delta\Delta E^{\ddagger}$ and $\Delta\Delta G^{\ddagger}$ calculated by each functional could be a consequence of the small differences in the transition structure geometries, since this geometry depends on the functional used for the optimization. Therefore, it is interesting to quantify how similar the structures are. We have used the minimized RMSD deviations between the structures for each pair of functionals, and have also compared the differences between the set of redundant internal coordinates generated by the Gaussian03 program.[51] The dihedral angles in which three consecutive atoms form an angle smaller than 15° were excluded, since, in this case, small changes in the position of one atom implied large and meaningless differences in the dihedral angle. Even though most bond distances and angles are listed in the set of internal coordinates, the distance corresponding to the bonds that are forming (or breaking) in the transition state is usually not included. As this is an important parameter in a transition state, we also analyzed selected distances following an analysis of the imaginary frequencies in the transition states.

The results of these comparisons are shown in Fig. 7, 8, and 9. We compared the differences in geometrical parameters between each possible pair of functionals. The average (top-right) and maximum (bottom-left part of each table) of the 38 structures (nineteen reactions and two competing transition states for each reaction) is represented.

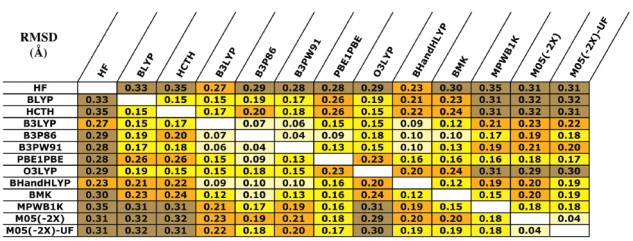

Fig. 7 Mean value of the average RMSD deviation (in Å) for all transition structures with each pair of methods.

The values shown in Fig. 7, 8, and 9 reveal that HF transition structures are the most distinctive of all the methods. Pure GGA functionals (BLYP and HCTH) also show large differences to hybrid-GGA and meta-GGA functionals, and the deviations between BLYP and HCTH are smaller. With the exception of O3LYP, hybrid-GGA functionals usually give similar geometries to the hybrid meta-GGA functionals, although larger differences were observed for the dihedral angles. The transition states'

Bond distance deviation (Å)

	HF	BLYP	HCTH	B3LYP	B3P86	B3PW91	PBE1PBE	O3LYP	BHandHLYP	BMK	MPWB1K	M05(-2X)	M05(-2X)-UF
HF		0.03	0.02	0.02	0.02	0.02	0.02	0.02	0.01	0.02	0.02	0.02	0.02
BLYP	0.23		0.01	0.01	0.02	0.02	0.02	0.02	0.03	0.02	0.03	0.02	0.02
HCTH	0.19	0.09		0.01	0.01	0.01	0.01	0.00	0.02	0.01	0.02	0.01	0.01
B3LYP	0.18	0.09	0.09		0.01	0.01	0.01	0.00	0.01	0.01	0.02	0.01	0.01
B3P86	0.22	0.14	0.14	0.08		0.00	0.00	0.01	0.01	0.01	0.01	0.01	0.01
B3PW91	0.20	0.12	0.12	0.06	0.02		0.00	0.01	0.01	0.01	0.01	0.01	0.01
PBE1PBE	0.21	0.15	0.14	0.09	0.02	0.03		0.01	0.01	0.01	0.01	0.01	0.01
O3LYP	0.19	0.10	0.05	0.07	0.10	0.08	0.11		0.02	0.01	0.02	0.01	0.01
BHandHLYP	0.13	0.16	0.15	0.08	0.10	0.10	0.10	0.13		0.01	0.01	0.01	0.01
BMK	0.18	0.16	0.15	0.09	0.08	0.07	0.07	0.12	0.08		0.02	0.01	0.01
MPWB1K	0.20	0.18	0.18	0.11	0.09	0.09	0.08	0.15	0.09	0.07		0.01	0.01
M05(-2X)	0.20	0.17	0.16	0.11	0.08	0.09	0.08	0.14	0.09	0.08	0.08		0.00
M05(-2X)-UF	0.20	0.17	0.16	0.11	0.08	0.09	0.08	0.14	0.09	0.08	0.09	0.01	

Bond (breaking or forming) distance deviation (Å)

	HF	BLYP	HCTH	B3LYP	B3P86	B3PW91	PBE1PBE	O3LYP	BHandHLYP	BMK	MPWB1K	M05(-2X)	M05(-2X)-UF
HF		0.15	0.12	0.11	0.14	0.13	0.14	0.12	0.08	0.12	0.12	0.13	0.13
BLYP	0.25		0.06	0.06	0.09	0.08	0.10	0.06	0.10	0.10	0.11	0.11	0.11
HCTH	0.21	0.08		0.06	0.08	0.07	0.09	0.03	0.10	0.10	0.10	0.10	0.10
B3LYP	0.19	0.09	0.08		0.05	0.04	0.06	0.04	0.05	0.05	0.06	0.07	0.07
B3P86	0.24	0.13	0.12	0.07		0.01	0.01	0.06	0.07	0.05	0.05	0.05	0.05
B3PW91	0.22	0.12	0.10	0.06	0.02		0.02	0.05	0.06	0.04	0.05	0.05	0.05
PBE1PBE	0.23	0.14	0.12	0.08	0.02	0.03		0.06	0.07	0.04	0.05	0.05	0.05
O3LYP	0.21	0.09	0.05	0.07	0.09	0.07	0.09		0.08	0.07	0.08	0.08	0.08
BHandHLYP	0.14	0.16	0.15	0.08	0.11	0.11	0.11	0.13		0.05	0.05	0.06	0.06
BMK	0.19	0.15	0.14	0.07	0.07	0.07	0.07	0.11	0.07		0.03	0.05	0.05
MPWB1K	0.19	0.16	0.15	0.08	0.08	0.08	0.08	0.12	0.07	0.05		0.05	0.05
M05(-2X)	0.21	0.15	0.15	0.10	0.08	0.08	0.08	0.12	0.09	0.07	0.07		0.00
M05(-2X)-UF	0.21	0.16	0.15	0.10	0.08	0.08	0.08	0.12	0.09	0.07	0.07	0.00	

Fig. 8 Mean value of the average (top-right) and maximum (bottom-left) bond distance deviation (table above) and forming or breaking bond distance (bottom table) for each pair of methods, in Å.

Angle deviation (degrees)

	HF	BLYP	HCTH	B3LYP	B3P86	B3PW91	PBE1PBE	O3LYP	BHandHLYP	BMK	MPWB1K	M05(-2X)	M05(-2X)-UF
HF		1.1	1.0	0.8	0.9	0.9	0.9	0.8	0.5	0.9	0.9	0.9	0.9
BLYP	8.7		0.4	0.4	0.7	0.6	0.7	0.5	0.7	0.8	0.9	0.9	0.9
HCTH	7.9	3.2		0.5	0.6	0.6	0.7	0.3	0.7	0.8	0.9	0.9	0.9
B3LYP	6.8	3.2	3.6		0.3	0.3	0.4	0.3	0.4	0.5	0.6	0.6	0.6
B3P86	8.3	5.0	5.1	2.8		0.1	0.1	0.5	0.5	0.4	0.4	0.5	0.5
B3PW91	7.8	4.4	4.3	2.1	1.0		0.2	0.4	0.4	0.4	0.5	0.5	0.5
PBE1PBE	8.2	5.6	5.4	3.5	1.1	1.8		0.5	0.5	0.4	0.4	0.4	0.4
O3LYP	7.3	3.7	2.1	2.6	3.9	3.0	4.5		0.6	0.7	0.8	0.7	0.7
BHandHLYP	5.1	5.6	5.6	2.8	3.9	3.5	4.1	4.5		0.5	0.5	0.5	0.5
BMK	7.6	5.7	5.9	3.4	2.8	3.0	2.9	4.8	3.5		0.3	0.5	0.4
MPWB1K	7.7	6.7	6.7	4.2	3.3	3.5	3.0	5.7	3.9	2.5		0.4	0.4
M05(-2X)	7.7	6.5	6.6	4.5	3.6	3.8	3.5	5.7	3.9	3.7	2.9		0.1
M05(-2X)-UF	7.9	6.6	6.8	4.6	3.6	3.8	3.5	5.8	4.0	3.6	3.0	0.5	

Dihedral angle deviation (degrees)

	HF	BLYP	HCTH	B3LYP	B3P86	B3PW91	PBE1PBE	O3LYP	BHandHLYP	BMK	MPWB1K	M05(-2X)	M05(-2X)-UF
HF		4.9	4.8	3.6	4.1	3.9	4.0	3.9	2.8	4.0	4.3	3.9	3.9
BLYP	33.3		1.6	1.9	2.7	2.4	3.2	2.3	3.1	3.3	4.0	4.2	4.2
HCTH	33.3	10.2		2.1	2.7	2.4	3.1	1.7	3.0	3.4	3.9	4.1	4.1
B3LYP	26.4	11.7	14.7		1.1	0.9	1.6	1.5	1.4	1.8	2.4	2.8	2.7
B3P86	28.4	14.9	17.0	5.0		0.5	0.7	1.9	1.8	1.5	1.9	2.3	2.2
B3PW91	27.9	14.1	15.9	4.1	2.4		1.0	1.5	1.7	1.7	2.1	2.4	2.3
PBE1PBE	27.2	18.3	18.6	9.5	5.4	6.4		2.2	2.0	1.7	1.7	2.0	2.0
O3LYP	28.1	13.8	13.2	9.6	11.3	9.3	12.5		2.3	2.7	3.2	3.2	3.2
BHandHLYP	23.0	17.9	19.1	7.3	9.0	8.8	12.3	14.5		2.0	2.5	2.2	2.1
BMK	27.4	19.1	20.9	9.4	8.0	9.1	11.2	16.2	10.3		1.5	2.3	2.2
MPWB1K	29.9	21.1	22.9	12.6	10.5	11.4	10.8	18.7	13.5	9.0		2.1	2.1
M05(-2X)	25.0	22.0	22.2	14.3	12.4	13.0	11.4	17.4	12.1	13.8	13.2		0.5
M05(-2X)-UF	25.1	21.8	21.8	13.9	12.0	12.6	11.0	17.5	11.8	13.1	13.0	2.3	

Fig. 9 Mean value of the average (top-right) and maximum (bottom-left) angle deviation (table above) and dihedral angle deviation (bottom table) for each pair of methods, in degrees.

forming and breaking bonds showed more variation than the other bonds.

The hybrid-GGA functionals show small average deviations for the parameters compared, but, as in the case of the energy differences, high individual errors might be hidden in these average values. To check this, we have analyzed the frequencies at which the highest deviations of a structural parameter for each transition state is over a threshold. We used the minimized RMSD, the dihedral angles and the distances of forming and breaking bonds. The results are shown in Fig. 10, 11 and 12.

The data shown in these figures shows that the HF or pure GGA methods analyzed give rather different results for transition

	HF	BLYP	HCTH	B3LYP	B3P86	B3PW91	PBE1PBE	O3LYP	BHANDHLYP	BMK	MPWB1K	M05(-2X)	M05(-2X)-UF
HF		12	11	8	11	11	11	12	6	11	15	12	12
BLYP	8		5	5	5	5	6	5	8	8	13	11	11
HCTH	7	2		3	7	4	8	2	6	11	13	10	10
B3LYP	6	3	2		0	1	1	3	1	4	11	9	9
B3P86	6	5	2	0		1	1	7	3	3	7	7	5
B3PW91	6	5	2	0	0		2	4	3	6	10	9	9
PBE1PBE	7	5	2	1	1	1		10	2	2	5	5	4
O3LYP	6	3	2	1	1	1	2		9	11	14	12	11
BHANDHLYP	6	4	2	0	0	0	1	1		4	11	5	5
BMK	6	4	2	0	0	1	1	4	0		7	8	6
MPWB1K	7	6	4	1	1	2	0	6	1	1		10	11
M05(-2X)	7	6	4	3	2	3	2	4	3	3	2		0
M05(-2X)-UF	7	7	4	3	2	3	2	5	3	2	2	0	

Fig. 10 Times that RMSD differences were higher than 0.2 Å (top-right) and 0.4 Å (bottom-left).

	HF	BLYP	HCTH	B3LYP	B3P86	B3PW91	PBE1PBE	O3LYP	BHANDHLYP	BMK	MPWB1K	M05(-2X)	M05(-2X)-UF
HF		18	15	17	18	18	20	16	14	18	18	17	17
BLYP	4		4	5	12	11	13	5	12	15	13	10	11
HCTH	2	1		8	11	10	11	2	14	14	10	10	10
B3LYP	3	2	0		6	3	9	6	5	6	8	8	9
B3P86	5	2	0	0		0	0	10	9	7	8	7	7
B3PW91	3	2	0	0	0		0	8	9	5	5	4	4
PBE1PBE	5	2	0	0	0	0		11	9	6	5	6	5
O3LYP	2	2	0	0	0	0	0		13	11	10	10	10
BHANDHLYP	1	2	1	0	2	1	2	1		5	4	9	10
BMK	3	2	0	0	0	0	0	0	0		2	8	8
MPWB1K	3	2	1	0	0	0	0	0	0	0		3	2
M05(-2X)	4	2	1	0	0	0	0	1	0	0	0		0
M05(-2X)-UF	4	2	1	0	0	0	0	1	0	0	0	0	

Fig. 11 Times that maximum deviations distances of bonds forming (or breaking) in the TS were higher than 0.1 Å (top-right) and 0.4 Å (bottom-left).

	HF	BLYP	HCTH	B3LYP	B3P86	B3PW91	PBE1PBE	O3LYP	BHANDHLYP	BMK	MPWB1K	M05(-2X)	M05(-2X)-UF
HF		6	7	6	6	6	7	6	6	6	6	7	7
BLYP	2		1	2	3	2	3	2	4	5	6	5	5
HCTH	3	0		2	2	2	2	2	3	5	5	4	5
B3LYP	2	0	1		0	0	1	1	1	3	5	4	5
B3P86	2	0	1	0		0	1	1	1	1	4	4	4
B3PW91	2	0	1	0	0		1	0	1	4	4	4	4
PBE1PBE	2	1	2	0	0	0		2	2	2	2	4	4
O3LYP	2	1	1	0	0	0	0		2	4	6	4	5
BHANDHLYP	2	0	1	0	0	0	0	0		3	5	4	3
BMK	2	0	1	0	0	0	0	0	0		2	5	5
MPWB1K	2	1	2	0	0	0	0	0	0	0		6	6
M05(-2X)	2	1	2	0	0	0	0	0	0	0	0		0
M05(-2X)-UF	2	1	2	0	0	0	0	0	0	0	0	0	

Fig. 12 Times that maximum dihedral angle deviations were higher than 30° (top-right) and 90° (bottom-left).

state geometry optimizations than the geometries from hybrid meta-GGA functionals. In Fig. 13, examples of the deviations of the transition state structures optimized with HF and with M05-(-2X)-UF are given. The results are not better for some pure GGA structures.

Hybrid-GGA functionals give geometries that are closer to the most sophisticated models, but in some cases the differences are rather large. For example, for B3LYP, in three (out of thirty-eight) transition structures the RMSD was higher than 0.4 Å and in one transition structure the maximum dihedral angle deviation was greater than 60° (see ESI†). In nine transition structures the maximum difference for the forming bonds compared to the structures optimized by M05(-2X)-UF were higher than 0.1 Å. However, the results obtained with BMK or MPWB1K functionals with respect to M05(-2X)-UF are not much closer

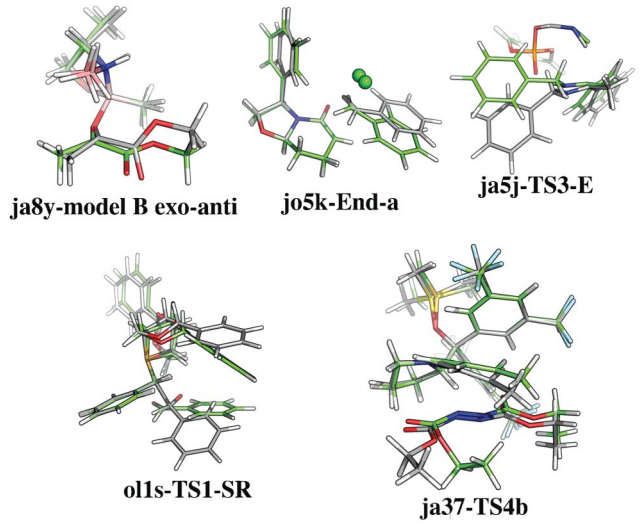

Fig. 13 Comparison of the structures optimized with HF (gray) and M05(-2X)-UF (green) methods for some of the TS studied.

to M05(-2X)-UF, and PBE1PBE, a hybrid-GGA functional, also gives similar results.

Combined use of different functionals for geometry optimization and for single-point calculation

All the results reported so far have used the same level of theory throught the calculation, and we call this "*Method 1*". The similarities between the geometries calculated by hybrid GGA functionals and hybrid meta GGA functionals suggest that it may be an effective strategy to use hybrid GGA functionals in geometry optimizations, followed by a single-point energy evaluation using a more expensive hybrid meta GGA functional ("*Method 2*"). The calculation of $\Delta\Delta E^{\ddagger}$ is straightforward using this approach. For $\Delta\Delta G^{\ddagger}$, however, there is a choice: should vibrational frequencies be calculated using the higher or the lower level of theory? Fig. 3 illustrates that $\Delta\Delta G^{\ddagger}$ is sensitive even to a change from a fine to an ultrafine grid. Since the calculation of vibrational frequencies is only valid at stationary points on the potential energy surface, we have chosen the level of theory used for geometry optimisation to calculate the vibrational correction.

- *Method 1*: Entire calculation at specified level of theory
- *Method 2*: As *Method 1*, but with an additional single-point calculation using M05(-2X)-UF (Gaussian03 keyword: integral = grid = ultrafine) on the method 1 geometry.

For $\Delta\Delta E^{\ddagger}$: M05(-2X)-UF single-point energy is used.

For $\Delta\Delta G^{\ddagger}$: the difference between the values for $\Delta\Delta E^{\ddagger}$ calculated using *Method 1* and *Method 2* is added to the $\Delta\Delta G^{\ddagger}$ value calculated using *Method 1*.

This approach avoids the use of the ultrafine grid during the optimization stage, which greatly increases the computational time.

To assess the accuracy of *Method 2*, we have re-evaluated the $\Delta\Delta E^{\ddagger}$ and $\Delta\Delta G^{\ddagger}$, using the structures optimized with each functional, but evaluating the energy with the M05(-2X) functional and the ultrafine grid. For $\Delta\Delta G^{\ddagger}$ evaluation the single-point energy calculated with M05(-2X) functional was added to the correction to the Gibbs free energy calculated with the same level of theory used in the optimization step. Like all the other functionals, M05(-2X) is an approximate functional, so its results are not as precise as extrapolated methods.[89–100] Nevertheless, these systems are too large to be studied by these, or other, high-quality methods. Tests on M05(-2X) demonstrate that these functionals offer quite accurate results for thermodynamic properties, kinetic properties,[14,38,40,41,68,69] medium-range intearactions[8,19,38] and intermolecular interactions.[7,41,68,69] Therefore M05(-2X) DFT is probably the most reliable of the methods available in the Gaussian03 program, that can be applied to structures of the size of those in the Fig. 2.

The results of *Method 2* are summarized in Fig. 14. For each reaction, the differences in $\Delta\Delta E^{\ddagger}$ (top) and $\Delta\Delta G^{\ddagger}$ (middle) calculated from the geometries optimized for each functional, with respect to the values obtained from the M05(-2X)-UF optimized structures are shown. To facilitate comparison, the differences between the $\Delta\Delta E^{\ddagger}$ obtained by the same functional used in the optimization and $\Delta\Delta E^{\ddagger}$ calculated with the M05(-2X)-UF optimized structure (*Method 1*) is also shown in the table in the bottom.

The data in Fig. 14 reveal average differences of over 1 kcal/mol when the $\Delta\Delta E^{\ddagger}$ was calculated using the same method employed in the optimization (*Method 1*). However, these differences are reduced when energies are recalculated with the M05(-2X)-UF functional (*Method 2*). For HF and for the non-hybrid functionals tested, the average differences were around 1 kcal/mol, but it was reduced to less than 0.5 kcal/mol when geometries optimized by hybrid-GGA functionals were used. The O3LYP functional is an exception. It has been observed that the Gaussian03 rev. C implementation of this functional is not able to reproduce the atomization energies published in the original O3LYP functional,[101] and it was corrected in rev. D of the program. Some studies report that the performance of O3LYP functional is similar or superior to B3LYP,[102,103] even though in some cases these tests were done using the "old" Gaussian03 implementation.[104,105] In our hands, however, the results obtained with the latter version of this functional in Gaussian03 are the least effective of the hybrid-GGA functionals. It is of particular interest that average differences obtained for PBE1PBE, B3P86 and BHandHLYP functionals were smaller. Remarkably, the other hybrid meta-GGA functionals tested (BMK and MPWB1K) show similar deviations as these hybrid-GGA functionals with respect to M05-(-2X)-UF.

The results of $\Delta\Delta E^{\ddagger}$ calculations with M05(-2X) functionals were very similar when the ultrafine or standard grids were used in the transition state optimization. In the worst case, the difference was smaller than 0.3 kcal/mol. However, when the Gibbs free energy correction is added to calculate $\Delta\Delta G^{\ddagger}$, large differences are observed. This is in agreement with previous observation in the unreliability of Gibbs free energy correction evaluation when hybrid meta-GGA functionals are used with the standard grid. Interestingly, the differences in $\Delta\Delta G^{\ddagger}$ are higher for the hybrid meta-GGA functionals used with standard grid than for any of the hybrid GGA functionals, with the exception of O3LYP.

From these comparisons, the use of hybrid GGA functionals, such as B3LYP, with a standard grid in transition state geometry optimization followed by single-point evaluation of the energy using a more sophisticated functional with the ultrafine grid (in this paper M05-2X) seems quite appropriate for most applications. To further illustrate this point, we have recalculated the results in

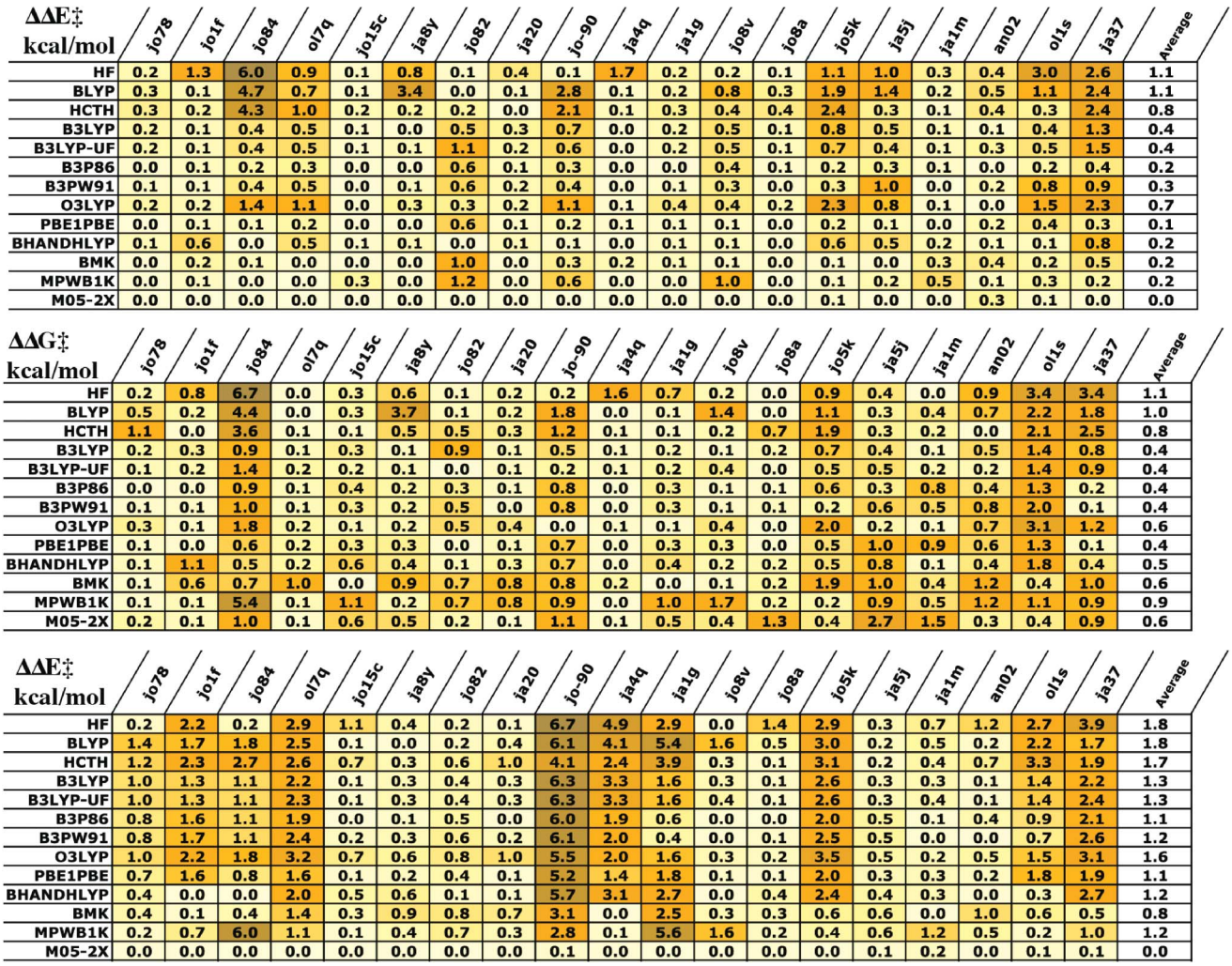

ΔΔE‡ kcal/mol	jo78	jo1f	jo84	ol7q	jo15c	ja8y	jo82	ja20	jo-90	ja4q	ja1g	jo8v	jo8a	jo5k	ja5j	ja1m	an02	ol1s	ja37	Average
HF	0.2	1.3	6.0	0.9	0.1	0.8	0.1	0.4	0.1	1.7	0.2	0.2	0.1	1.1	1.0	0.3	0.4	3.0	2.6	1.1
BLYP	0.3	0.1	4.7	0.7	0.1	3.4	0.0	0.1	2.8	0.1	0.2	0.8	0.3	1.9	1.4	0.2	0.5	1.1	2.4	1.1
HCTH	0.3	0.2	4.3	1.0	0.2	0.2	0.2	0.0	2.1	0.1	0.3	0.4	0.4	2.4	0.3	0.1	0.4	0.3	2.4	0.8
B3LYP	0.2	0.1	0.4	0.5	0.1	0.0	0.5	0.3	0.7	0.0	0.2	0.5	0.1	0.8	0.5	0.1	0.1	0.4	1.3	0.4
B3LYP-UF	0.2	0.1	0.4	0.5	0.1	0.1	1.1	0.2	0.6	0.0	0.2	0.5	0.1	0.7	0.4	0.1	0.3	0.5	1.5	0.4
B3P86	0.0	0.1	0.2	0.3	0.0	0.0	0.6	0.1	0.3	0.0	0.0	0.4	0.1	0.2	0.3	0.1	0.0	0.2	0.4	0.2
B3PW91	0.1	0.1	0.4	0.5	0.0	0.1	0.6	0.2	0.4	0.0	0.1	0.3	0.0	0.3	1.0	0.0	0.2	0.8	0.9	0.3
O3LYP	0.2	0.2	1.4	1.1	0.0	0.3	0.3	0.2	1.1	0.1	0.4	0.4	0.2	2.3	0.8	0.1	0.0	1.5	2.3	0.7
PBE1PBE	0.0	0.1	0.1	0.2	0.0	0.0	0.6	0.1	0.2	0.1	0.1	0.1	0.0	0.2	0.1	0.0	0.2	0.4	0.3	0.1
BHANDHLYP	0.1	0.6	0.0	0.5	0.1	0.1	0.0	0.1	0.1	0.0	0.1	0.1	0.0	0.6	0.5	0.2	0.1	0.1	0.8	0.2
BMK	0.0	0.2	0.1	0.0	0.0	0.0	1.0	0.0	0.3	0.2	0.1	0.1	0.0	0.1	0.0	0.3	0.4	0.2	0.5	0.2
MPWB1K	0.0	0.1	0.0	0.0	0.3	0.0	1.2	0.0	0.6	0.0	0.0	1.0	0.0	0.1	0.2	0.5	0.1	0.3	0.2	0.2
M05-2X	0.0	0.0	0.0	0.0	0.0	0.0	0.0	0.0	0.0	0.0	0.0	0.0	0.0	0.1	0.0	0.0	0.3	0.1	0.0	0.0

ΔΔG‡ kcal/mol	jo78	jo1f	jo84	ol7q	jo15c	ja8y	jo82	ja20	jo-90	ja4q	ja1g	jo8v	jo8a	jo5k	ja5j	ja1m	an02	ol1s	ja37	Average
HF	0.2	0.8	6.7	0.0	0.3	0.6	0.1	0.2	0.2	1.6	0.7	0.2	0.0	0.9	0.4	0.0	0.9	3.4	3.4	1.1
BLYP	0.5	0.2	4.4	0.0	0.3	3.7	0.1	0.2	1.8	0.0	0.1	1.4	0.0	1.1	0.3	0.4	0.7	2.2	1.8	1.0
HCTH	1.1	0.0	3.6	0.1	0.1	0.5	0.5	0.3	1.2	0.1	0.1	0.2	0.7	1.9	0.3	0.2	0.0	2.1	2.5	0.8
B3LYP	0.2	0.3	0.9	0.1	0.3	0.1	0.9	0.1	0.5	0.1	0.2	0.1	0.2	0.7	0.4	0.1	0.5	1.4	0.8	0.4
B3LYP-UF	0.1	0.2	1.4	0.2	0.2	0.1	0.0	0.1	0.2	0.1	0.2	0.4	0.0	0.5	0.5	0.2	0.2	1.4	0.9	0.4
B3P86	0.0	0.0	0.9	0.1	0.4	0.2	0.3	0.1	0.8	0.0	0.3	0.1	0.1	0.6	0.3	0.8	0.4	1.3	0.2	0.4
B3PW91	0.1	0.1	1.0	0.1	0.3	0.2	0.5	0.0	0.8	0.0	0.3	0.1	0.1	0.2	0.6	0.5	0.8	2.0	0.1	0.4
O3LYP	0.3	0.1	1.8	0.2	0.1	0.2	0.5	0.4	0.0	0.1	0.1	0.4	0.0	2.0	0.2	0.1	0.7	3.1	1.2	0.6
PBE1PBE	0.1	0.0	0.6	0.2	0.3	0.3	0.0	0.1	0.7	0.0	0.3	0.3	0.0	0.5	1.0	0.9	0.6	1.3	0.1	0.4
BHANDHLYP	0.1	1.1	0.5	0.2	0.6	0.4	0.1	0.3	0.7	0.0	0.4	0.2	0.2	0.5	0.8	0.1	0.4	1.8	0.4	0.5
BMK	0.1	0.6	0.7	1.0	0.0	0.9	0.7	0.8	0.8	0.2	0.0	0.1	0.2	1.9	1.0	0.4	1.2	0.4	1.0	0.6
MPWB1K	0.1	0.1	5.4	0.1	1.1	0.2	0.7	0.8	0.9	0.0	1.0	1.7	0.2	0.2	0.9	0.5	1.2	1.1	0.9	0.9
M05-2X	0.2	0.1	1.0	0.1	0.6	0.5	0.2	0.1	1.1	0.1	0.5	0.4	1.3	0.4	2.7	1.5	0.3	0.4	0.9	0.6

ΔΔE‡ kcal/mol	jo78	jo1f	jo84	ol7q	jo15c	ja8y	jo82	ja20	jo-90	ja4q	ja1g	jo8v	jo8a	jo5k	ja5j	ja1m	an02	ol1s	ja37	Average
HF	0.2	2.2	0.2	2.9	1.1	0.4	0.2	0.1	6.7	4.9	2.9	0.0	1.4	2.9	0.3	0.7	1.2	2.7	3.9	1.8
BLYP	1.4	1.7	1.8	2.5	0.1	0.0	0.2	0.4	6.1	4.1	5.4	1.6	0.5	3.0	0.2	0.5	0.2	2.2	1.7	1.8
HCTH	1.2	2.3	2.7	2.6	0.7	0.3	0.6	1.0	4.1	2.4	3.9	0.3	0.1	3.1	0.2	0.4	0.7	3.3	1.9	1.7
B3LYP	1.0	1.3	1.1	2.2	0.1	0.3	0.4	0.3	6.3	3.3	1.6	0.3	0.1	2.6	0.3	0.3	0.1	1.4	2.2	1.3
B3LYP-UF	1.0	1.3	1.1	2.3	0.1	0.3	0.4	0.3	6.3	3.3	1.6	0.4	0.1	2.6	0.3	0.4	0.1	1.4	2.4	1.3
B3P86	0.8	1.6	1.1	1.9	0.0	0.1	0.5	0.0	6.0	1.9	0.6	0.0	0.0	2.0	0.5	0.1	0.4	0.9	2.1	1.1
B3PW91	0.8	1.7	1.1	2.4	0.2	0.3	0.6	0.2	6.1	2.0	0.4	0.0	0.1	2.5	0.5	0.0	0.0	0.7	2.6	1.2
O3LYP	1.0	2.2	1.8	3.2	0.7	0.6	0.8	1.0	5.5	2.0	1.6	0.3	0.2	3.5	0.5	0.2	0.5	1.5	3.1	1.6
PBE1PBE	0.7	1.6	0.8	1.6	0.1	0.2	0.4	0.1	5.2	1.4	1.8	0.1	0.1	2.0	0.3	0.3	0.2	1.8	1.9	1.1
BHANDHLYP	0.4	0.0	0.0	2.0	0.5	0.6	0.1	0.1	5.7	3.1	2.7	0.0	0.4	2.4	0.4	0.3	0.0	0.3	2.7	1.2
BMK	0.4	0.1	0.4	1.4	0.3	0.9	0.8	0.7	3.1	0.0	2.5	0.3	0.3	0.6	0.6	0.0	1.0	0.6	0.5	0.8
MPWB1K	0.2	0.7	6.0	1.1	0.1	0.4	0.7	0.3	2.8	0.1	5.6	1.6	0.2	0.4	0.6	1.2	0.5	0.2	1.0	1.2
M05-2X	0.0	0.0	0.0	0.0	0.0	0.0	0.0	0.0	0.1	0.0	0.0	0.0	0.0	0.0	0.1	0.2	0.0	0.1	0.1	0.0

Fig. 14 Absolute differences (kcal/mol) in $\Delta\Delta E^{\ddagger}$ (top) and $\Delta\Delta G^{\ddagger}$ (middle) calculated using M05(-2X)-UF functionals on geometries found with each functional (*Method 2*) with respect to the values obtained from the M05(-2X)-UF optimized structures, in kcal/mol. To facilitate comparison, the absolute difference in $\Delta\Delta E^{\ddagger}$ obtained by the same functional using (*Method 1*), with respect to M05(-2X)-UF, is given at the bottom.

Fig. 3 using the $\Delta\Delta E^{\ddagger}$ and $\Delta\Delta G^{\ddagger}$ calculated with this *Method 2* (Fig. 15). The new graphics illustrates that B3LYP for geometry optimization followed by M05-2X-UF single-point evaluation is an effective method for the calculation of $\Delta\Delta E^{\ddagger}$. Other hybrid GGA functionals as B3P86 and PBE1PBE shows comparable or better results, but despite the relatively small average differences, the maximum differences are sometimes large. For example for B3LYP, B3P86 and PBE1PBE functionals, at least in three of the reactions studied, the deviations in the single-point energy difference with respect to M05(-2X)-UF were greater than 0.5 kcal/mol. HF and pure GGA functionals, however, seem not to be precise enough to obtain reliable TS geometries.

Of particular importance is the observation that the calculation of $\Delta\Delta G^{\ddagger}$ B3LYP (hybrid GGA) transition structure geometries lead to better results than hybrid meta GGA functionals using the standard grid, mainly due to the unreliability of the frequency analysis. This is quite clear in Fig. 15 (bottom).

Finally, *Method 2* also generates $\Delta\Delta G^{\ddagger}$ that are similar to the values obtained experimentally. This is shown in Fig. 16 where the differences with respect to experimental values of $\Delta\Delta G^{\ddagger}$ are shown for both *Method 1* and *Method 2*. *Method 2* gives the correct enantioselectivity for the jo5k reaction, in contrast to Fig. 4 where the single-point energy was calculated using the same functionals as the geometry optimization.

Summary

Theoretical studies of organic reaction are limited by the computer power available, and so compromises must usually be made between reducing the level of theory, or simplifying the molecules. Our analyses suggest:

(i) Geometries from HF and pure GGA functionals should be avoided.

(ii) Vibrational free energy corrections obtained with meta-GGA functionals and standard grids are misleading in many cases.

(iii) TS geometries obtained by hybrid GGA functionals are similar to those obtained by meta-GGA functionals, but seem to be less sensitive to the grid. However, the single-point energies are less accurate.

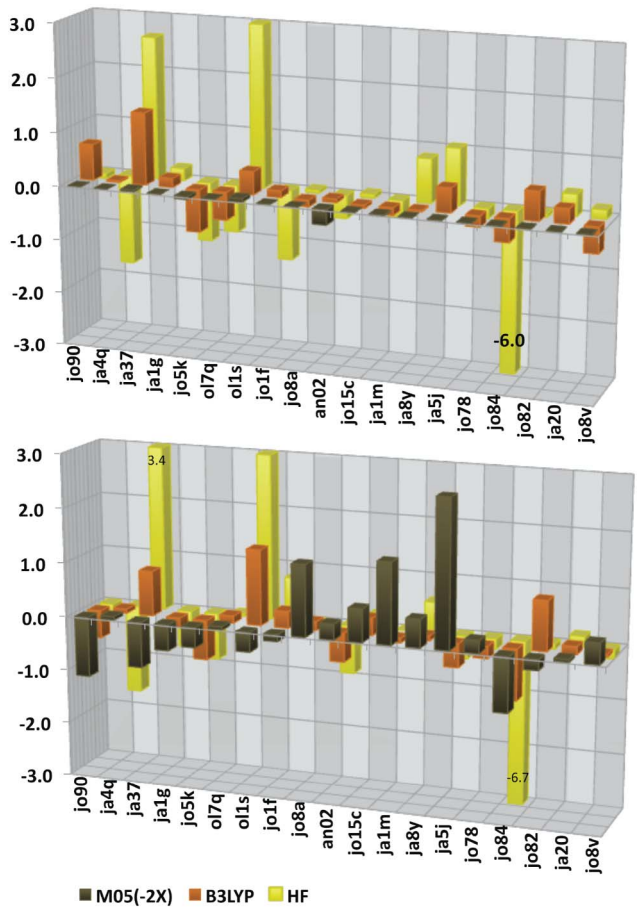

Fig. 15 Comparison of $\Delta\Delta E^{\ddagger}$ (top) and $\Delta\Delta G^{\ddagger}$ (bottom) for each pair of competing transition states with respect to values obtained with M05(-2X)-UF for HF, B3LYP and M05(-2X) using *Method 2* (see text).

(iv) Geometry optimization by meta-GGA functionals using ultrafine integration grids are probably the most reliable methods that can be used today for DFT calculations. However, these functionals are computationally more demanding than hybrid GGA functionals and the use of ultrafine grids redoubles the computational costs.

(v) The use of hybrid GGA functionals (such as B3LYP) in the geometry optimization step and the Gibbs free energy correction terms followed by single-point energy evaluation using meta-GGA functional (such as M05-2X) offers a good compromise between accuracy and computational cost. The use of an ultrafine grid does not make a big difference to this process, even in the final single-point calculation. The most demanding part of the calculation is done with the cheapest method.

Recommendation

We recommend the use of *Method 2* but with a default grid throughout: first optimise geometries and calculate a Gibbs free energy correction with B3LYP (default grid); then find a single-point energy with M05-2X. This single-point energy is a more reliable result that the corresponding B3LYP energy; the B3LYP Gibbs free energy correction should be added to the M05-2X single-point energy to obtain the overall Gibbs free energy.

	method 1	method 2
HF	0.9	0.5
BLYP	0.9	0.9
HCTH	1.1	1.0
B3LYP	1.0	0.7
B3LYP-UF	0.8	0.6
B3P86	0.9	0.6
B3PW91	1.0	0.7
PBE1PBE	0.9	0.6
O3LYP	1.1	0.9
BHANDHLYP	0.9	0.6
BMK	1.2	1.0
MPWB1K	0.8	0.8
M05-2X	0.8	0.7
M05-2X-UF	0.4	0.4

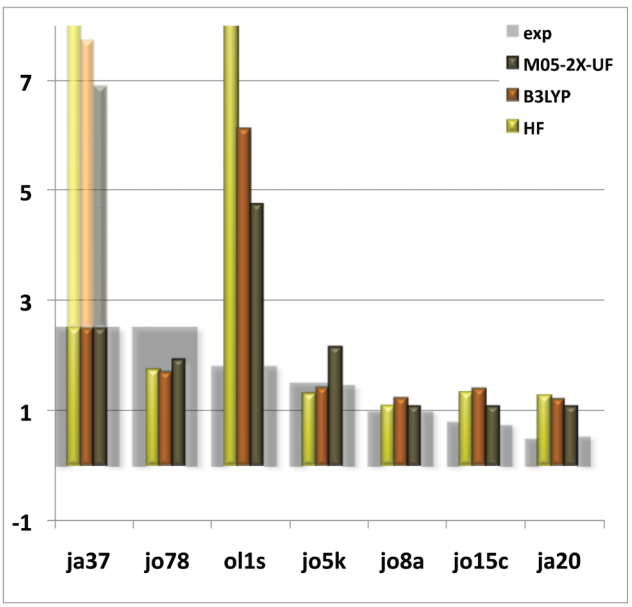

Fig. 16 Top: average absolute differences between $\Delta\Delta G^{\ddagger}$ calculated and deduced from experiments, in kcal/mol. Bottom, individual values for HF, B3LYP and M05(-2X)-UF (*Method 2*).

Conclusions

The $\Delta\Delta E^{\ddagger}$ and $\Delta\Delta G^{\ddagger}$ values obtained with some popular DFT functionals have been analyzed for a set of nineteen organic reactions, using two competing transition structures for each. Geometry optimization and frequency calculation by hybrid GGA functionals, (*e.g.* B3LYP), followed by a single-point calculation using a hybrid meta-GGA functional (*e.g.* M05-2X), gives reasonably good results compared with transition states optimized with the more expensive hybrid meta-GGA functionals. Similar geometries are obtained by both methods. However, geometry optimization using one functional followed by single-point frequency calculation using another does not generally yield acceptable results.

In conclusion, therefore, hybrid GGA functionals such as B3LYP, still have an important role to play in the search for transition state geometries for organic reactions, and can generate results that are almost as reliable as much more expensive computational methods once they have been combined with single-point energy calculations using more modern hybrid meta-functionals.

Acknowledgements

This research was supported by a Marie Curie Intra-European Fellowship within the 6th European Community Framework Programme MEIF-CT2006-040554. The authors would like to acknowledge the use of CamGrid service in carrying out this work.

Notes and references

1 W. Koch and M. C. Holthausen, *A chemist's guide to Density functional Theory*, Wiley-VCH, Weinheim, 2000.
2 R. G. Parr and W. Yang, *Density Functional Theory of Atoms and Molecules*, Oxford University Press, Oxford, 1989.
3 A. H. Zewail, *Femtochemistry: Ultrafast Dynamics of the Chemical Bond*, World Scientific Publishing Company, Singapore, 1994.
4 A. D. Becke, *J. Chem. Phys.*, 1993, **98**, 5648–5652.
5 C. Lee, W. Yang and R. G. Parr, *Phys. Rev. B: Condens. Matter*, 1988, **37**, 785.
6 M. D. Wodrich, C. Corminboeuf and P. v. R. Schleyer, *Org. Lett.*, 2006, **8**, 3631–3634.
7 Y. Zhao and D. G. Truhlar, *J. Chem. Theory Comput.*, 2006, **3**, 289–300.
8 Y. Zhao and D. G. Truhlar, *Org. Lett.*, 2006, **8**, 5753–5755.
9 Y. Zhao and D. G. Truhlar, *J. Phys. Chem. A*, 2006, **110**, 10478–10486.
10 C. E. Check and T. M. Gilbert, *J. Org. Chem.*, 2005, **70**, 9828–9834.
11 E. I. Izgorodina, D. R. B. Brittain, J. L. Hodgson, E. H. Krenske, C. Y. Lin, M. Namazian and M. L. Coote, *J. Phys. Chem. A*, 2007, **111**, 10754–10768.
12 S. N. Pieniazek, F. R. Clemente and K. N. Houk, *Angew. Chem., Int. Ed.*, 2008, **47**, 7746–7749.
13 S. Grimme, M. Steinmetz and M. Korth, *J. Org. Chem.*, 2007, **72**, 2118–2126.
14 T. A. Rokob, A. Hamza and I. Papai, *Org. Lett.*, 2007, **9**, 4279–4282.
15 S. Grimme, M. Steinmetz and M. Korth, *J. Chem. Theory Comput.*, 2006, **3**, 42–45.
16 P. R. Schreiner, A. A. Fokin, R. A. Pascal and A. de Meijere, *Org. Lett.*, 2006, **8**, 3635–3638.
17 G. Stefan, *Angew. Chem., Int. Ed.*, 2006, **45**, 4460–4464.
18 P. R. Schreiner, *Angew. Chem., Int. Ed.*, 2007, **46**, 4217–4219.
19 G. I. Csonka, A. Ruzsinszky, J. P. Perdew and S. Grimme, *J. Chem. Theory Comput.*, 2008, **4**, 888–891.
20 W. Paul and C. Timothy, *J. Comput. Chem.*, 2004, **25**, 725–733.
21 Y. Zhao and D. G. Truhlar, *J. Chem. Theory Comput.*, 2005, **1**, 415–432.
22 Y. Zhao and D. G. Truhlar, *Phys. Chem. Chem. Phys.*, 2005, **7**, 2701–2705.
23 Y. Zhao and D. G. Truhlar, *J. Phys. Chem. A*, 2004, **108**, 6908–6918.
24 H. Zhao and D. G. Truhlar, *Theor Chem Acta*, 2007.
25 J. Tao, J. P. Perdew, V. N. Staroverov and G. E. Scuseria, *Phys. Rev. Lett.*, 2003, **91**, 146401.
26 V. N. Staroverov, G. E. Scuseria, J. Tao and J. P. Perdew, *J. Chem. Phys.*, 2003, **119**, 12129–12137.
27 J. Toulouse, A. Savin and C. Adamo, *J. Chem. Phys.*, 2002, **117**, 10465–10473.
28 Y. Zhao, B. J. Lynch and D. G. Truhlar, *J. Phys. Chem. A*, 2004, **108**, 4786–4791.
29 T. Schwabe and S. Grimme, *Phys. Chem. Chem. Phys.*, 2007, **9**, 3397–3406.
30 T. Schwabe and S. Grimme, *Acc. Chem. Res.*, 2008, **41**, 569–579.
31 S. Grimme, *J. Comput. Chem.*, 2006, **27**, 1787–1799.
32 S. Grimme, J. Antony, T. Schwabe and C. Mück-Lichtenfeld, *Org. Biomol. Chem.*, 2007, **5**, 741–758.
33 G. T. de Jong and F. M. Bickelhaupt, *J. Phys. Chem. A*, 2005, **109**, 9685–9699.
34 E. I. Izgorodina, M. L. Coote and L. Radom, *J. Phys. Chem. A*, 2005, **109**, 7558–7566.
35 M. M. Quintal, A. Karton, M. A. Iron, A. D. Boese and J. M. L. Martin, *J. Phys. Chem. A*, 2005, **110**, 709–716.
36 Y. Zhao, N. Gonzalez-Garcia and D. G. Truhlar, *J. Phys. Chem. A*, 2005, **109**, 2012–2018.
37 E. A. Amin and D. G. Truhlar, *J. Chem. Theory Comput.*, 2007, **4**, 75–85.
38 M. D. Wodrich, C. Corminboeuf, P. R. Schreiner, A. A. Fokin and P. v. R. Schleyer, *Org. Lett.*, 2007, **9**, 1851–1854.
39 B. R. White, C. R. Wagner, D. G. Truhlar and E. A. Amin, *J. Chem. Theory Comput.*, 2008, **4**, 1718–1732.
40 Y. Zhao and D. G. Truhlar, *J. Phys. Chem. A*, 2008, **112**, 1095–1099.
41 Y. Zhao and D. G. Truhlar, *Acc. Chem. Res.*, 2008, **41**, 157–358.
42 Y. Zhao and D. G. Truhlar, *J. Chem. Theory Comput.*, 2009, **5**, 324–333.
43 A. Dkhissi, J. M. Ducéré, R. Blossey and C. Pouchan, *J. Comput. Chem.*, 2009, **30**, 1179–1184.
44 M. Korth and S. Grimme, *J. Chem. Theory Comput.*, 2009, **5**, 993–1003.
45 J. Zheng, Y. Zhao and D. G. Truhlar, *J. Chem. Theory Comput.*, 2006, **3**, 569–582.
46 O. Tishchenko, J. Zheng and D. G. Truhlar, *J. Chem. Theory Comput.*, 2008, **4**, 1208–1219.
47 B. J. Lynch and D. G. Truhlar, *J. Phys. Chem. A*, 2001, **105**, 2936–2941.
48 G. O. Jones, V. A. Guner and K. N. Houk, *J. Phys. Chem. A*, 2005, **110**, 1216–1224.
49 V. Guner, K. S. Khuong, A. G. Leach, P. S. Lee, M. D. Bartberger and K. N. Houk, *J. Phys. Chem. A*, 2003, **107**, 11445–11459.
50 K. Yang, J. Zheng, Y. Zhao and D. G. Truhlar, *J. Chem. Phys.*, 2010, **132**, 164117–164110.
51 P. Chunyang, Y. A. Philippe, H. B. Schlegel and J. F. Michael, *J. Comput. Chem.*, 1996, **17**, 49–56.
52 L. Goerigk and S. Grimme, *J. Chem. Theory Comput.*, 2010, **6**, 107–126.
53 A. D. Boese and J. M. L. Martin, *J. Chem. Phys.*, 2003, **119**, 3006–3014.
54 N. X. Wang and A. K. Wilson, *J. Chem. Phys.*, 2004, **121**, 7632–7646.
55 N. X. Wang, K. Venkatesh and A. K. Wilson, *J. Phys. Chem. A*, 2005, **110**, 779–784.
56 N. X. Wang and A. K. Wilson, *Mol. Phys.*, 2005, **103**, 345–358.
57 B. P. Prascher, B. R. Wilson and A. K. Wilson, *J. Chem. Phys.*, 2007, **127**, 124110–124114.
58 M. J. Frisch, *et al.*, *Gaussian 03, Revision E.01, Gaussian, Inc.*, Wallingford, CT, 2004.
59 A. D. Becke, *Phys. Rev. A: At., Mol., Opt. Phys.*, 1988, **38**, 3098.
60 A. D. Boese, N. L. Doltsinis, N. C. Handy and M. Sprik, *J. Chem. Phys.*, 2000, **112**, 1670–1678.
61 A. D. Boese and N. C. Handy, *J. Chem. Phys.*, 2001, **114**, 5497–5503.
62 P. J. Stephens, F. J. Devlin, C. F. Chabalowski and M. J. Frisch, *J. Phys. Chem.*, 2002, **98**, 11623–11627.
63 A. J. Cohen and N. C. Handy, *Mol. Phys.*, 2001, **99**, 607–615.
64 N. C. Handy and A. J. Cohen, *Mol. Phys.*, 2001, **99**, 403–412.
65 J. P. Perdew, K. Burke and M. Ernzerhof, *Phys. Rev. Lett.*, 1996, **77**, 3865–3868.
66 C. Adamo and V. Barone, *J. Chem. Phys.*, 1999, **110**, 6158–6171.
67 A. D. Boese and J. M. L. Martin, *J. Chem. Phys.*, 2004, **121**, 3405–3416.
68 Y. Zhao, N. E. Schultz and D. G. Truhlar, *J. Chem. Theory Comput.*, 2006, **2**, 364–382.
69 Y. Zhao, N. E. Schultz and D. G. Truhlar, *J. Chem. Phys.*, 2005, **123**, 161103–161104.
70 A. Arrieta, F. P. Cossio and B. Lecea, *J. Org. Chem.*, 2001, **66**, 6178–6180.
71 A. G. Moglioni, E. Muray, J. A. Castillo, A. Alvarez-Larena, G. Y. Moltrasio, V. Branchadell and R. M. Ortuno, *J. Org. Chem.*, 2002, **67**, 2402–2410.
72 M. Cui, W. Adam, J. H. Shen, X. M. Luo, X. J. Tan, K. X. Chen, R. Y. Ji and H. L. Jiang, *J. Org. Chem.*, 2002, **67**, 1427–1435.
73 M. Freccero, R. Gandolfi, M. Sarzi-Amade and A. Rastelli, *J. Org. Chem.*, 2002, **68**, 811–823.
74 J. Li, W.-Y. Jiang, K.-L. Han, G.-Z. He and C. Li, *J. Org. Chem.*, 2003, **68**, 8786–8789.
75 R. W. Alder, S. P. East, J. N. Harvey and M. T. Oakley, *J. Am. Chem. Soc.*, 2003, **125**, 5375–5387.
76 W. Harb, M. F. Ruiz-Lopez, F. Coutrot, C. Grison and P. Coutrot, *J. Am. Chem. Soc.*, 2004, **126**, 6996–7008.
77 R. J. Nielsen, J. M. Keith, B. M. Stoltz and W. A. Goddard, *J. Am. Chem. Soc.*, 2004, **126**, 7967–7974.
78 M. A. Silva, B. R. Bellenie and J. M. Goodman, *Org. Lett.*, 2004, **6**, 2559–2562.
79 W. H. Lam, P. P. Gaspar, D. A. Hrovat, D. A. Trieber, E. R. Davidson and W. T. Borden, *J. Am. Chem. Soc.*, 2005, **127**, 9886–9894.
80 F. R. Clemente and K. N. Houk, *J. Am. Chem. Soc.*, 2005, **127**, 11294–11302.

81 A. Fu, B. List and W. Thiel, *J. Org. Chem.*, 2005, **71**, 320–326.
82 R. S. Paton and J. M. Goodman, *Org. Lett.*, 2006, **8**, 4299–4302.
83 S. Bertelsen, M. Marigo, S. Brandes, P. Diner and K. A. Jorgensen, *J. Am. Chem. Soc.*, 2006, **128**, 12973–12980.
84 C. T. Wong and M. W. Wong, *J. Org. Chem.*, 2007, **72**, 1425–1430.
85 M. N. Paddon-Row, L. C. H. Kwan, A. C. Willis and M. S. Sherburn, *Angew. Chem., Int. Ed.*, 2008, **47**, 7013–7017.
86 I. Soteras, O. Lozano, C. Escolano, M. Orozco, M. Amat, J. Bosch and F. J. Luque, *J. Org. Chem.*, 2008, **73**, 7756–7763.
87 L. Simón and J. M. Goodman, *J. Am. Chem. Soc.*, 2009, **131**, 4070–4077.
88 C. Gourlaouen, G. Ujaque, A. Lledos, M. Medio-Simon, G. Asensio and F. Maseras, *J. Org. Chem.*, 2009, **74**, 4049–4054.
89 A. Tajti, P. G. Szalay, A. G. Csaszar, M. Kallay, J. Gauss, E. F. Valeev, B. A. Flowers, J. Vazquez and J. F. Stanton, *J. Chem. Phys.*, 2004, **121**, 11599–11613.
90 Y. J. Bomble, J. Vazquez, M. Kallay, C. Michauk, P. G. Szalay, A. G. Csaszar, J. Gauss and J. F. Stanton, *J. Chem. Phys.*, 2006, **125**, 064108–064108.
91 A. Karton, E. Rabinovich, J. M. L. Martin and B. Ruscic, *J. Chem. Phys.*, 2006, **125**, 144108–144117.
92 D. Kats, T. Korona and M. Schutz, *J. Chem. Phys.*, 2007, **127**, 064107–064112.
93 J. A. Pople, M. Head-Gordon, D. J. Fox, K. Raghavachari and L. A. Curtiss, *J. Chem. Phys.*, 1989, **90**, 5622–5629.
94 L. A. Curtiss, C. Jones, G. W. Trucks, K. Raghavachari and J. A. Pople, *J. Chem. Phys.*, 1990, **93**, 2537–2545.
95 L. A. Curtiss, K. Raghavachari, G. W. Trucks and J. A. Pople, *J. Chem. Phys.*, 1991, **94**, 7221–7230.
96 L. A. Curtiss, K. Raghavachari, P. C. Redfern, V. Rassolov and J. A. Pople, *J. Chem. Phys.*, 1998, **109**, 7764–7776.
97 L. A. Curtiss, P. C. Redfern and K. Raghavachari, *J. Chem. Phys.*, 2007, **126**, 084108–084112.
98 L. A. Curtiss, K. Raghavachari and J. A. Pople, *J. Chem. Phys.*, 1993, **98**, 1293–1298.
99 L. A. Curtiss, P. C. Redfern, K. Raghavachari, V. Rassolov and J. A. Pople, *J. Chem. Phys.*, 1999, **110**, 4703–4709.
100 L. A. Curtiss, P. C. Redfern and K. Raghavachari, *J. Chem. Phys.*, 2007, **127**, 124105–124108.
101 Y. Zhao, J. Pu, B. J. Lynch and D. G. Truhlar, *Phys. Chem. Chem. Phys.*, 2004, **6**, 673–676.
102 J. Baker and P. Pulay, *J. Comput. Chem.*, 2003, **24**, 1184–1191.
103 J. Baker and P. Pulay, *J. Chem. Phys.*, 2002, **117**, 1441–1449.
104 V. A. Guner, K. S. Khuong, K. N. Houk, A. Chuma and P. Pulay, *J. Phys. Chem. A*, 2004, **108**, 2959–2965.
105 T. Strassner and M. A. Taige, *J. Chem. Theory Comput.*, 2005, **1**, 848–855.

